Chemical Engineering Journal 292 (2016) 389–397

Contents lists available at ScienceDirect

Chemical Engineering Journal

journal homepage: www.elsevier.com/locate/cej

Aqueous arsenic (As) and antimony (Sb) removal by potassium ferrate

Bingyan Lan, Yingxin Wang, Xi Wang *, Xueting Zhou, Yuan Kang, Laisheng Li *

Guangdong Engineering Technology Research Center for Drinking Water Safety, School of Chemistry & Environment, South China Normal University, Guangzhou 510006, China

HIGHLIGHTS

- Fe(VI) removed As and Sb individually and simultaneously from solution effectively.
- IR and XRD defined the amorphous characterization of DP/Ferrate.
- Synergistic effect on simultaneous sorption of As and Sb by DP/Ferrate were found.
- IR and XPS demonstrated the presence of arsenato antimonates.
- Configuration of the adsorbed As and Sb speciation onto DP/Ferrate was postulated.

GRAPHICAL ABSTRACT

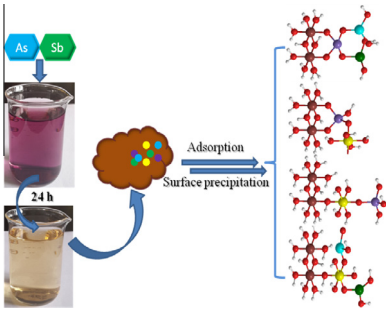

ARTICLE INFO

Article history:
Received 5 December 2015
Received in revised form 5 February 2016
Accepted 6 February 2016
Available online 9 February 2016

Keywords:
Arsenic
Antimony
Ferrate (VI) decay product
Adsorption
Mechanism

ABSTRACT

Priority pollutants arsenic (As) and antimony (Sb) were removed from aqueous solution by potassium ferrate. As(III) and Sb(III) were oxidized, then separated from solution by the adsorption of Fe(VI) decay product (DP/Ferrate). XRD and FTIR results revealed the "amorphous" characteristics of DP/Ferrate. Adsorption studies in single-solute and bi-solute systems were conducted. The maximum adsorption capacity (Q_{max}) of single As was 162.02 mg $(g\ K_2FeO_4)^{-1}$ at pH_0 6.5 and of single Sb was 129.93 mg $(g\ K_2FeO_4)^{-1}$ at pH_0 4.0. Regarding bi-solute adsorption, a synergistic effect between As and Sb was demonstrated. Compared to single-solute adsorption, the adsorption rates of both elements were enhanced significantly. The adsorption isotherm of Sb in the presence of As was reproduced well by the Brunauer–Emmett–Teller (BET) model, indicating heterogeneous multilayer adsorption. The FTIR spectra featured the appearances of new peaks compared to the blank spectrum of DP/Ferrate, indicating that the surface speciation contained Fe–O–As and Fe–O–Sb bonds in the corresponding single-solute system; As–O–Sb binding was found in the bi-solute system. Furthermore, high-resolution XPS analysis pointed to the formation of arsenato antimonates of a polymer-like configuration, which was believed to account for the synergistic effect on simultaneous adsorption of As and Sb by DP/Ferrate. This paper demonstrated that using potassium ferrate is a viable water treatment technology to remediate arsenic and antimony combined pollution.

1. Introduction

Arsenic and antimony are metalloids but are usually classified as heavy metals. According to a recent research survey [1], 26 million people throughout West Bengal and 80 million people in Bangladesh have been exposed to toxic levels of As-contaminated groundwater. More than 1.0×10^5 tons of antimony is reported to be consumed worldwide each year [2]. As a result, anthropogenic emission causes the Sb concentration in soil and natural waters to greatly exceed its baseline concentration [3]. Due to severe environmental contamination and its consequences to human

* Corresponding authors. Tel.: +86 20 39310185; fax: +86 20 39319187.
E-mail addresses: wangxi@m.scnu.edu.cn (X. Wang), llsh@scnu.edu.cn (L. Li).

http://dx.doi.org/10.1016/j.cej.2016.02.019
1385-8947/

health, arsenic and antimony are both considered pollutants of priority interest by the European Union [4] and by the Environmental Protection Agency of the United States [5].

Arsenic and antimony belong to the same group in the periodic chart and share similar chemical properties. They commonly present together (e.g., in Sb-ores [6] and copper electrorefining solution [7]). In natural soils and the aqueous environment, both occur as oxyanions either in the pentavalent (V) state in oxic environments or the trivalent (III) state in anoxic environments. Their speciations are strongly controlled by redox potential and pH [8,9]. In the pH range 4–9, As(V) most exists as $H_2AsO_4^-$ and $HAsO_4^{2-}$ whereas As(III) usually occurs as uncharged H_3AsO_3. For pH > 2.7 $H_2SbO_4^-$ and $Sb(OH)_6^-$ are predominant under oxidizing conditions while in the pH range 2.7–10.4 uncharged $Sb(OH)_3$ dominates under reducing conditions. The US EPA has lowered the maximum contaminant level (MCL) of As and Sb in drinking water to 10 μg/L and 5 μg/L, respectively [9]. The more stringent MCL along with the severe contamination crisis occurring worldwide have driven researchers and authorities to upgrade treatment technologies to remove arsenic and antimony from waste streams.

One promising method is to use the iron coprecipitation/adsorption process. As(III) and As(V) sorption onto ferrihydrite, goethite, lepidocrocite, akaganeite, schwertmannite and hematite have been well documented [10–17]. Prior studies have demonstrated As(III) and As(V) adsorption on iron oxides through the formation of inner-sphere surface complexes via ligand exchange with OH_2 and/or OH^- groups on the iron oxide surface [18]. Zhang et al. [19] confirmed that As(III) species formed bidentate and monodentate corner-sharing complexes with Fe(III) octahedra. The interaction mode of the As(V) species on iron oxide surfaces was studied by various spectroscopic techniques [20–22], providing strong evidence that adsorption occurs by the formation of bidentate edge or corner sharing between arsenate tetrahedra and FeO_6 octahedra. Compared to adsorption studies of arsenic, however, reports on antimony removal from water are limited. Scheiost et al. [23] carried out EXAFS analysis and demonstrated that Sb(III) and Sb(V) formed a bidentate mononuclear, corner-sharing inner-sphere complex at the goethite surface. Guo et al. [2] observed an analogous Sb–O coordination environment of Sb (V) sorbed on ferrihydrite. However, Mitsunobu et al. [24] detected the formation of a bidentate binuclear complex between Sb(V) and ferrihydrite, which Guo et al. [2] failed to obtain. Hence, the binding mechanism is still controversial.

Ferrate, being the highest valence state of iron, is regarded as a powerful and environmentally innocuous reagent for water/wastewater treatment [25]. It has a redox potential of 2.2 V at acidic pH, which is higher than other commonly used oxidants (e.g., ozone and permanganate) in water/wastewater treatment [26]. The resulting decomposition product is iron (III) oxyhydroxide, an excellent adsorbent/coagulant [27]. Beneficial as a result of its dual function, ferrate is effective in arsenic (III) oxidation and subsequent coagulation by its decomposition product [28]. Prucek et al. [29] further investigated the arsenic removal mechanism by potassium ferrate in water. They reported that the decomposition of potassium ferrate yielded γ-Fe_2O_3(core)/γ-FeOOH (shell) nanoparticles and that the adsorbed arsenic was embedded into the tetrahedral sites of γ-Fe_2O_3. To our knowledge, there has been only one study on the reaction of antimony with ferrate (VI) in water. Johnson and Lorenz [30] demonstrated the successful removal of Sb(III) to below MCL using a mixture of Fe(II) and Fe(VI).

The simultaneous removal of arsenic and antimony has been reported in studies [7,31] addressing the efficient removal of both elements. The mechanism behind the efficiency is of interest but still unknown. In the present study, potassium ferrate was used to remove arsenic and antimony from aqueous solution, strictly speaking, through oxidizing As(III) and Sb(III) to less-toxic As(V) and Sb(V), respectively, followed by adsorptive removal via the in-situ-formed ferrate decomposition product (referred as DP/Ferrate). Attention was paid to the differences of adsorption behavior of single As and Sb onto DP/Ferrate. In comparison to adsorption in the single-solute system, the simultaneous adsorption process of antimony and arsenic onto DP/Ferrate was investigated. To elucidate the bonding nature of adsorbed metals on the surface of DP/Ferrate in both single and bi-solute systems, Fourier transform infrared spectrometry (FTIR) and X-ray photoelectron spectroscopy (XPS) were used.

2. Materials and methods

2.1. Materials

The potassium ferrate (K_2FeO_4) used was synthesized in the laboratory according to the method of Delaude and Laszlo [32]. The purity was checked spectrophotometrically at 505 nm [28]. A molar absorption coefficient $\varepsilon_{505nm} = 1150\ M^{-1}\ cm^{-1}$ was used for the calculation of Fe(VI) concentration and a purity of 95% or above was confirmed for each experiment. Details of other chemicals and materials are provided in the Supplementary Material.

2.2. Experimental procedure

Batch experiments were carried out in a series of 250 mL stoppered Erlenmeyer flask. The general experimental procedure is described in the Supplementary Material. Adsorption studies in single-solute and bi-solute systems were conducted under carefully controlled conditions as described below.

2.2.1. Adsorption edge and effect of ionic strength

The effect of pH and ionic strength of the solution on the adsorption of single arsenic and antimony were studied in a single-solute system. The initial concentration of single As(III) or Sb(III) was fixed at 2 mg L^{-1}. The initial pH was varied between 3.5 and 6.5, and the ionic strength of the solution was varied between 0.001 M and 0.1 M. The dose of K_2FeO_4 used was 50 mg L^{-1}, equivalent to 14 mg L^{-1} Fe.

2.2.2. Adsorption kinetics

In the single-solute system, 100 mL As(III) solution which containing 0.01 M $NaNO_3$ background electrolyte, or 100 mL Sb(III) solution containing 0.001 and 0.01 M $NaNO_3$, was added to a series of flasks. The initial concentration of single As(III) or Sb(III) was 2 mg L^{-1}. A pH_0 of 6.5 was used for the arsenic kinetic study, and a pH_0 of 4.0 and 6.5 was used for the antimony kinetic study. The amount of K_2FeO_4 used was 50 mg L^{-1}. At desired time intervals, 5 mL aliquots were taken from the suspension. In bi-solute system, As(III) solution and Sb(III) solution was mixed to obtained a 100 mL reaction volume. The concentration of each element in the final solution was 1 mg L^{-1}, thus the total toxic ion concentration was 2 mg L^{-1}. The pH_0 was set to 4.0 and 6.5, and the ionic strength was set to 0.01 M and 0.001 M $NaNO_3$. The applied dose of K_2FeO_4 and the sampling manner were the same as those used in the single-solute system.

2.2.3. Adsorption isotherm

In the single-solute system, a series of As(III) or Sb(III) solutions ranging from 1 to 10 mg L^{-1} were prepared to study the adsorption isotherm. The pH_0 was set to be 6.5 for arsenic adsorption and 4.0 for antimony adsorption. In the bi-solute system, the initial concentration of As(III) was fixed at 1 mg L^{-1} whereas the initial concentration of Sb(III) varied from 0.1 to 3 mg L^{-1}. The pH_0 was 4.0. In both systems, the applied dose of K_2FeO_4 was fixed to 50 mg L^{-1},

the ionic strength was maintained at 0.01 M and an equilibrium time of 24 h was used.

2.3. Analysis and characterization

2.3.1. Spectroscopic characterization

Powder X-ray diffraction (XRD) was used to characterize the DP/Ferrate sample. FTIR was used to investigate the bonding structure of adsorbed As and Sb species on DP/Ferrate. XPS was performed to verify the oxidation state and speciation on the surface of DP/Ferrate. The sample preparation, detailed equipment types and measurement procedure are described in the Supplementary Material.

2.3.2. Analysis

The concentration of As_{total} and Sb_{total} in the collected samples was determined by inductively coupled plasma atomic emission spectroscopy (ICP-AES) (iCAP 6500 Duo, Thermo Scientific). Solution pH measurements were conducted using a pH meter (PHS-3C, Shanghai INESA Scientific Instrument Co. Ltd.) and a combined pH electrode (E-201-C) that provided a precision of ±0.01 pH.

2.4. Theory

2.4.1. Kinetic models

The evolution of the adsorption capacity with time was modeled by pseudo-second-order and intra-particle diffusion rate equations.

2.4.2. Adsorption isotherms

In the single-solute system, sorption isotherms were modeled using two-parameter isotherm models (the Langmuir model and Freundlich models) and a three-parameter adsorption isotherm model (the Langmuir–Freundlich model). In the bi-solute system, the Brunauer–Emmett–Teller (BET) isotherm model was adopted. Non-linear regression analysis was employed to fit the isotherm models to sorption data.

Expressions corresponding to these kinetic and isotherm models are listed in the Supplementary Material.

3. Results and discussions

3.1. Characterization of decomposition product of K_2FeO_4

The XRD pattern of DP/Ferrate is shown in Fig. 1. Two very broad peaks at 2θ values of approximately 35 and 62 degrees were found. Through comparison with standard diffractograms, these can be assigned to 2-line ferrihydrite, which is the least crystalline form of iron (hydr)oxide [33].

For detecting functional groups of DP/Ferrate, infrared spectroscopy was used. Infrared transmittance spectra are shown in Fig. 2(a). An intense and broad band centered at 3400 cm^{-1} is attributed to the stretching vibrations of OH groups associated with Fe atoms in DP/Ferrate [34]. A solitary band of H_2O-bending located at 1630 cm^{-1} was observed and was considerably weaker than OH-stretching bands [34]. IR bands at 1479 and 1364 cm^{-1} revealed the presence of NO_3^- and CO_3^{2-} in the DP/Ferrate sample [35,36]. The bands occurring near 460–600 cm^{-1} indicated Fe^{3+}–O^{2-} vibrational transitions, which was typical for low-crystalline ferrihydrite [36].

The XRD patterns and IR spectra of the DP/Ferrate sample matched the characteristics of "amorphous" ferrihydrite. Ferrihydrite is the initial product of Fe^{3+} hydrolysis in water and exhibits an extra-fine grain size of approximately 1.5–3.0 nm [37] and large specific surface area of 250–600 m^2/g [38]. In the structure of ferrihydrite, both octahedrally and tetrahedrally coordinated Fe atoms were found [39], resulting in the occurrence of "coordination-unsaturated" surface sites. These active surface sites, when combined with large surface area, make DP/Ferrate highly suitable for adsorption.

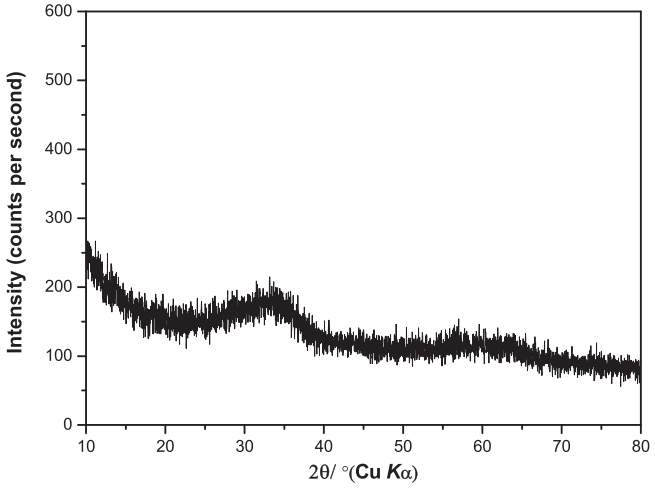

Fig. 1. XRD diffractogram of DP/Ferrate sample isolated from freeze-dried.

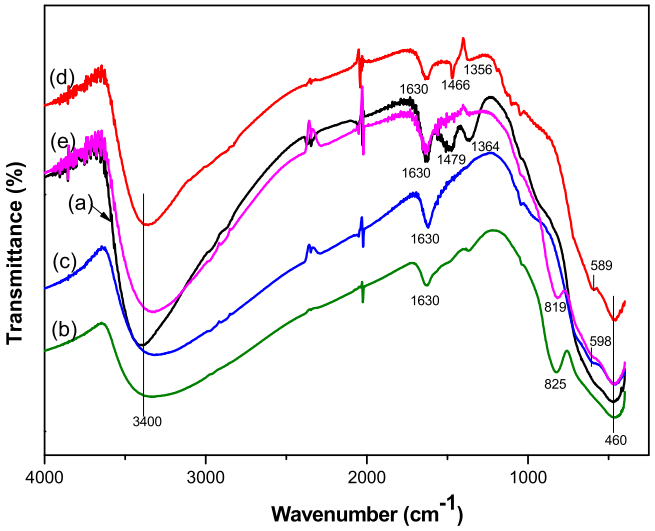

Fig. 2. FTIR spectra of As@DP/Ferrate, Sb@DP/Ferrate and (As + Sb)@DP/Ferrate samples in comparison with blank DP/Ferrate sample. Spectrum (a): blank DP/Ferrate sample; spectrum (b): As@DP/Ferrate at pH_0 6.5; spectrum (c): Sb@DP/Ferrate at pH_0 4.0; spectrum (d): Sb@DP/Ferrate at pH_0 6.5; spectrum (e): (As + Sb)@DP/Ferrate at pH_0 4.0.

3.2. Adsorption behavior of arsenic and antimony in the single-solute system

3.2.1. pH edge and effect of ionic strength study in the single-solute system

It was found that in alkaline conditions As(III) was oxidized to As(V) by Fe(VI) with a stoichiometry of 3:2 ([As(III)]:[Fe(VI)]) [28] and Sb(III) to Sb(V) with a stoichiometry of 2:1 ([Sb(III)]:[Fe(VI)]) [30]. The oxidation reaction was completed within seconds. Therefore, the use of 1 min pre-oxidation time was adequate for all cases in this study. The effects of pH and IS on the removal of single As and Sb by potassium ferrate are illustrated in Fig. 3(a) and (b), respectively. Increasing the IS from 0.001 M to 0.1 M did not significantly vary the As sorption%, indicating the formation of inner-sphere

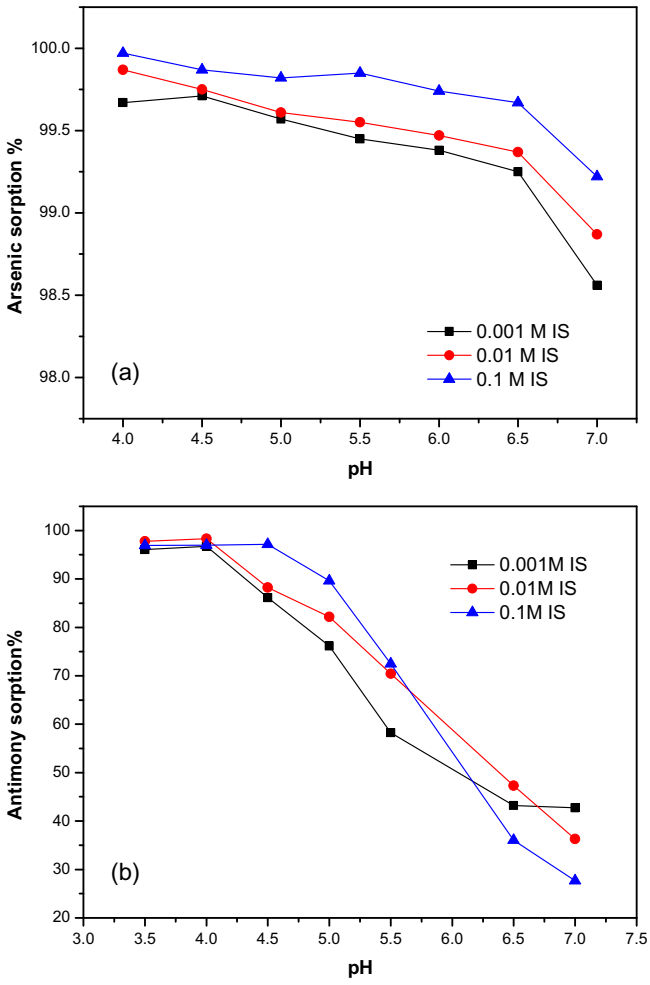

Fig. 3. Effect of pH and ionic strength on single (a) arsenic and (b) antimony sorption onto DP/Ferrate. $[As]_0$ or $[Sb]_0$ = 2 mg L^{-1}; K_2FeO_4 dose = 50 mg L^{-1}; 25 °C.

complexes on the surface of DP/Ferrate. Arsenic adsorption behavior under varied pH and IS were consistent with the reported patterns of other iron oxides [12,14,40]. Compared to arsenic, the pH dependence of antimony sorption on DP/Ferrate was more pronounced. Maximum sorption (above 96%) was found at the lowest studied pH_0 of 3.5 and decreased to 27% at pH_0 7.0. Over the tested pH range (3.5–7.0), the dominant form of Sb(V) in solution was $Sb(OH)_6^-$, and the sorption% of Sb(V) gradually dropped while moving toward the point of zero charge as the positive charge of DP/Ferrate surface decreased. As shown in Fig. 3(b), the IS dependency of Sb(V) adsorption on DP/Ferrate exhibited two opposite behaviors. In the pH range of 3.5–5.5, higher IS favored Sb(V) adsorption, whereas decreased Sb(V) adsorption with increasing IS was found in the pH range of 5.5–7.0. This behavior suggested the existence of two forms of surface complexes: an inner-sphere and an outer-sphere surface complex. A similar trend of pH and IS dependence on Sb (V) was obtained for various sorbents such as iron-oxide-rich red earth soils [41], goethite [42], and kaolinite [43]. McComb et al. [44] suggested that under acidic conditions Sb(V) was adsorbed onto the iron oxides through the formation of Fe–O–Sb bonds; in addition, across-surface antimonite oligomerization, such as $Sb_{12}(OH)_{64}^{4-}$, likely occurred to further stabilize the adsorbed Sb(V). At increased pH, the adsorbed Sb(V) oxyanion oligomers tended to be hydrolyzed to more readily desorbed monomers. In the present work, to elucidate the tendency of antimonite desorption at higher pH, Sb sorption% vs time was studied at pH_0 = 6.5; the results are

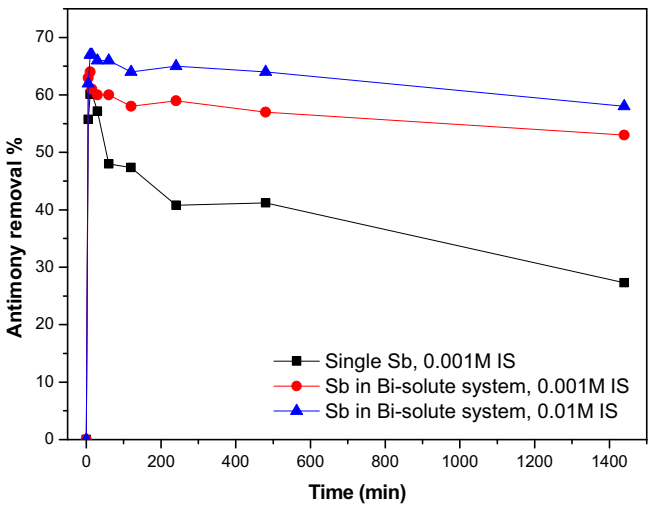

Fig. 4. Antimony removal% vs time in single and bi-solute system and under various IS. $[K_2FeO_4]$ = 50 mg L^{-1}; pH_0 = 6.5; 25 °C; (■): $[Sb]_0$ = 2 mg L^{-1}; IS = 0.001 M; (●): $[As]_0$ = 1 mg L^{-1}; $[Sb]_0$ = 1 mg L^{-1}; IS = 0.001 M; (▲): $[As]_0$ = 1 - mg L^{-1}; $[Sb]_0$ = 1 mg L^{-1}; IS = 0.01 M.

shown in Fig. 4. It can be observed that 60% of Sb was adsorbed rapidly in the first 15 min, followed by approximately 20% desorption, which is consistent with the results of McComb et al. [44].

3.2.2. Adsorption kinetics study in the single-solute system

The adsorption kinetics of arsenic was studied at pH_0 6.5. Additionally, the adsorption kinetics of antimony was conducted at pH_0 4.0 as a considerable desorption% was recorded at pH_0 6.5. A pseudo-second-order kinetic model was used to investigate the sorption mechanism of single arsenic and antimony onto DP/Ferrate particles (Fig. S1(a) and (b)). Fitted kinetic parameters are presented in Table 1. The values of correlation coefficient for both metals were extremely high (R^2 = 0.999), indicating that the pseudo-second-order model could describe the sorption process very well. The adsorption rate (k) of arsenic was 0.15 g mg^{-1} min^{-1}, which is 10 times higher than that of antimony (0.01 g $mg^{-1}min^{-1}$), indicating that arsenic had a higher binding affinity to the DP/Ferrate surface than antimony.

The strongly favored iron polymerization in amorphous DP/Ferrate [27] may lead to a complex porous configuration, which would provide both external and interior surface sites for adsorption. The possibility of intra-particle diffusion was elucidated using the intra-particle diffusion model.

Fig. S2(a) and (b) show the performance of the intra-particle diffusion kinetic model in describing the experimental data for both metals, in which data points are related by two straight lines. The first straight portion indicates that single arsenic and antimony overcame the external resistance and diffused onto the external surface of DP/Ferrate and the second represents intra-particle diffusion [45]. The values of rate parameters ($k_{id,1}$ and $k_{id,2}$) as well as the correlation coefficients are given in Table 1. The kinetic model indicates that in the first step arsenic much more rapidly equilibrates with the external sites than antimony, whereas in the second step antimony exhibited better mobility along the internal macropore walls.

3.2.3. Adsorption isotherm study in the single-solute system

Experimental equilibrium data and the goodness-of-fit of selected isotherm models are graphically shown in Fig. 5 (a) and (b) for single arsenic and antimony, respectively. Table 2 shows the isotherm parameters obtained using non-linear fitting analysis.

Table 1
Kinetic parameters for As and Sb adsorption onto DP/Ferrate, in both single solute and bi-solute system.

Metal	System	pH_0	k	q_e	r^2			
Pseudo-second-order model $\frac{t}{q_t}=\frac{1}{kq_e^2}+\left(\frac{1}{q_e}\right)t$								
As	Single	6.5	0.15	40.00	0.99			
Sb		4.0	0.01	39.68	0.99			
As	Bi-solute	6.5	0.60	19.92	1			
Sb		4.0	0.07	19.31	1			
Metal	System	pH_0	$k_{id,1}$	$k_{id,2}$	$k_{id,3}$	r_1^2	r_2^2	r_3^2
Intra-particle diffusion model $q_t=k_{id}t^{0.5}+I$								
As	Single	6.5	0.39	0.004	–	0.97	0.93	–
Sb		4.0	0.27	0.027	–	0.92	0.77	–
As	Bi-solute	6.5	0.40	0.004	–	0.88	0.95	–
Sb		4.0	2.64	0.150	3E−05	0.90	0.96	0.83

Arsenic sorption isotherms were obtained at pH_0 6.5. In terms of the two-parameter isotherm, the Freundlich model exhibited better representation (R^2 = 0.9805) of the experimental results than the Langmuir model (R^2 = 0.9269). The constant K_F value was found to be 82.32, indicating the high affinity of As to the DP/Ferrate surface. The K_F values of the three alternative adsorbents mesoporous iron manganese bimetal oxide [46], schwertmannite [47] and ferrihydrite [47] have been reported to be 15.659, 60.79 and 40.11, respectively. It is noted that the ferrihydrite synthesized by rapid titration of ferric nitrate had a K_F value (obtained at pH = 5.0) two times less than that of DP/Ferrate, suggesting that the DP/Ferrate underwent a higher degree of iron polymerization [27] that in turn increased specific surface area and porosity. The n value obtained from the Freundlich isotherm model was greater than 1, indicating the heterogeneity of binding sites of DP/Ferrate. Because the Freundlich isotherm could not model the saturation behavior, the Langmuir–Freundlich model was applied. According to the correlation coefficients in Table 2, the Langmuir–Freundlich isotherm was best able to describe our data. The calculated maximum adsorption capacity Q_{max} value of Langmuir–Freundlich model was 162.02 mg $(g\ K_2FeO_4)^{-1}$, which was higher than the value predicted from the Langmuir isotherm, implying that As(V) was adsorbed onto more than a monolayer of binding sites.

The single antimony adsorption isotherm was characterized at pH_0 4.0. The experimental data were found to follow the Freundlich and Langmuir–Freundlich isotherms with better accuracy than the Langmuir isotherm model (Table 2). The K_F value obtained in this work was 41.83 and n was found to be greater than 1, confirming that Sb(V) was adsorbed onto DP/Ferrate as a result of multilayer surface binding sites with heterogeneous affinity toward Sb (V). The value of Q_{max} obtained from the Langmuir–Freundlich model was 129.93 mg $(g\ K_2FeO_4)^{-1}$. Table 3 compares the Q_{max} of DP/Ferrate with other adsorbents, indicating the superior performance of DP/Ferrate in antimony adsorption.

3.3. Adsorption behavior of arsenic and antimony in the bi-solute (As + Sb) system

Phosphate, arsenic and antimony are in the same group 15 of the periodic table. Given the structural similarities among them, the presence of one could influence the adsorption of the other. Competition between arsenic and phosphorus on various adsorbents has been widely studied [17,52,53], but less attention has been paid to the coexistence of As and Sb in the adsorption reaction. Hence, the main purpose of this section is to discuss the adsorptive behavior of antimony in the presence of arsenic on DP/Ferrate.

3.3.1. Bi-solute (As + Sb) adsorption kinetics

The metal uptake% as a function of time was fitted with the pseudo-second-order kinetic model (Fig. S3) and the intra-particle diffusion model (Fig. S4) in the binary system of arsenic and antimony at two selected pH_0 values. The measure of goodness-of-fit (r^2) was extremely high (Table 1), confirming the satisfactory representation of the adsorption process by a pseudo-second-order kinetic expression. Comparing the single-

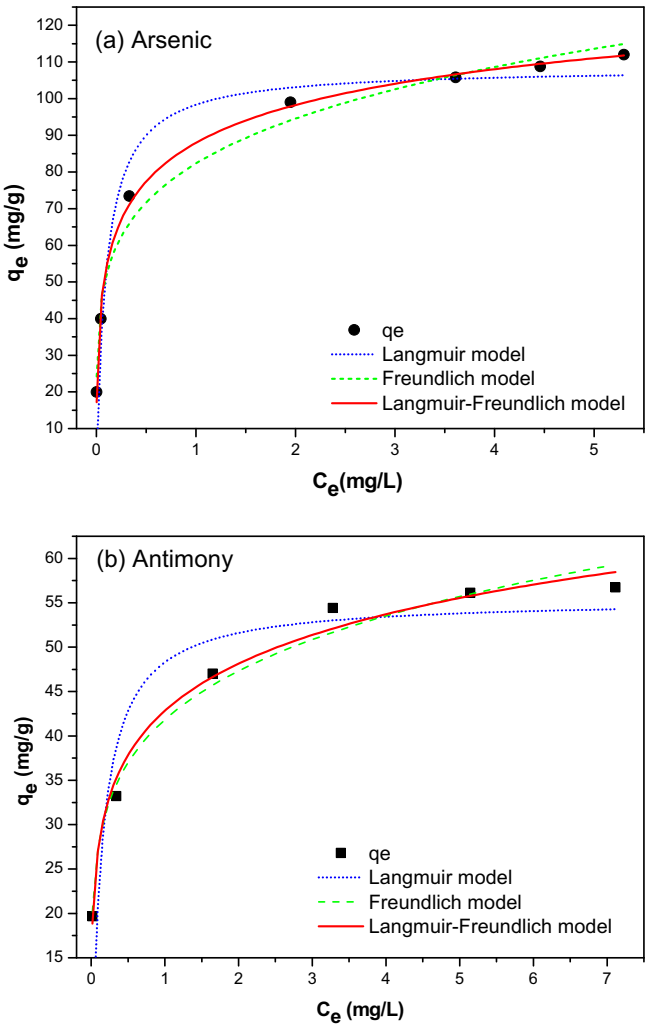

Fig. 5. Adsorption isotherms of (a) arsenic and (b) antimony on DP/Ferrate. $[As]_0$ or $[Sb]_0$ ranged from 1 to 10 mg L^{-1}; $[K_2FeO_4]$ = 50 mg L^{-1}; ionic strength = 0.01 M; pH_0 = 6.5 for arsenic adsorption and pH_0 = 4.0 for antimony adsorption, 25 °C.

Table 2
Constant parameters and correlation coefficients of various adsorption isotherm models for As and Sb adsorption onto DP/Ferrate in single and bi-solute system.

	Langmuir	Freundlich	Langmuir and Freundlich
Single As	Q_{max} = 108.41 mg g^{-1} K_L = 9.78 R^2 = 0.93	K_F = 82.32 n = 5 R^2 = 0.98	Q_{max} = 162.02 mg g^{-1} K_{LF} = 1.58 β = 0.38 R^2 = 0.99
Single Sb	Q_{max} = 55.38 mg g^{-1} K_L = 6.82 R^2 = 0.72	K_F = 41.83 n = 5.62 R^2 = 0.98	Q_{max} = 129.93 mg g^{-1} K_{LF} = 0.06 β = 0.25 R^2 = 0.98
Brunauer–Emmett–Teller isotherm model			
Sb in bi-solute system	q_s = 7.99 mg g^{-1} K_{BET} = 42.36 C_s = 0.07 mg L^{-1} R^2 = 0.94		

Table 3
Maximum adsorption capacities Q_{max} reported in literature in comparison with the one obtained in present work, for antimony removal from aqueous solutions.

Adsorbent	pH	Q_{max} (mg g^{-1})	Refs.
Ferric hydroxide	7.0	18.5	[48]
Fe–Mn binary oxide	5.0	120.53	[48]
Fe–Zr binary oxide	7.0	60.4	[49]
Synthetic manganite	3.0	95	[50]
Akaganeite	7.0	60.8	[51]
HFO	4.0	113.96	[2]
DP/Ferrate	4.0	129.93	Present work

solute (As or Sb) system to the bi-solute (As + Sb) system, the adsorption rate (k) of As was increased from 0.15 to 0.60 g mg^{-1} min^{-1} and k of Sb was increased from 0.01 to 0.07 g mg^{-1} min^{-1}. The significant improvement of adsorption rate in the bi-solute system demonstrated the occurrence of a synergistic promoting effect between arsenic and antimony. The kinetic data of arsenic were fitted with the intra-particle diffusion model, and two separate linear plots of q_t vs $t^{0.5}$ are presented in Fig. S4(a). It can be observed from Table 1 that the $k_{id,1}$ and $k_{id,2}$ of As did not differ considerably between the single-metal and bi-solute systems. The plot for antimony (Fig. S4(b)) featured three linear portions suggesting Sb diffused not only to macropores but also to mesopores and micropores of DP/Ferrate. The $k_{id,1}$ of Sb increased from 0.27 mg g^{-1} min$^{0.5}$ in the single-metal system to 2.64 mg g^{-1} min$^{0.5}$ when it was co-existed with As. Likewise, the value of $k_{id,2}$ increased from 0.03 to 0.15 mg g^{-1} min$^{0.5}$. The diffusion of antimony, both externally and internally, was significantly enhanced by the coexistence of arsenic. A very different adsorption behavior of antimony in the bi-solute system compared to the single-metal system was observed.

The time dependence of Sb sorption% in the bi-solute system at pH_0 = 6.5 is depicted in Fig. 4. Compared with the Sb uptake% in the single-metal system, the fraction of the desorbed Sb(V) decreased in the bi-solute system, indicating the formation of other type of bonds than Fe–O–Sb bonds. In addition, Fig. 4 illustrates the effect of ionic strength on the adsorption of Sb in the bi-solute system. An obvious improvement of sorption% at higher ionic strength was obtained, indicating the formation of inner-sphere surface complexes.

3.3.2. Bi-solute (As + Sb) adsorption isotherm

The antimony adsorption isotherm in the bi-solute system (Fig. 6) was analyzed at pH_0 = 4.0 and the initial arsenic concentration was fixed at 1 mg L^{-1}. According to the isotherm classification scheme suggested by Giles et al. [54], it can be classified within one of the sigmoidal-shaped (S) classes. The Brunauer–Emmett–Teller (BET) isotherm model was applied and developed to derive multi-layer adsorption onto non-homogeneous surfaces. Its validity in characterizing the equilibrium uptake for Sb in the bi-solute (As + Sb) system was demonstrated by the reasonably high correlation coefficient (R^2 = 0.94) estimated from non-linear fitting analysis (Table 2). As shown in Fig. 6, the inflection point at Ce = 0.07 mg L^{-1} suggested that the adsorption sites on the first layer of the DF/Ferrate surface were saturated by antimony. Beyond the inflection point, multi-layer adsorption occurred.

3.4. FTIR and XPS spectroscopic investigation

IR spectroscopy of DP/Ferrate samples before and after adsorption in both single and bi-solute systems, represented as As@DP/Ferrate, Sb@DP/Ferrate and (As + Sb)@DP/Ferrate, were analyzed. The results are illustrated in Fig. 2.

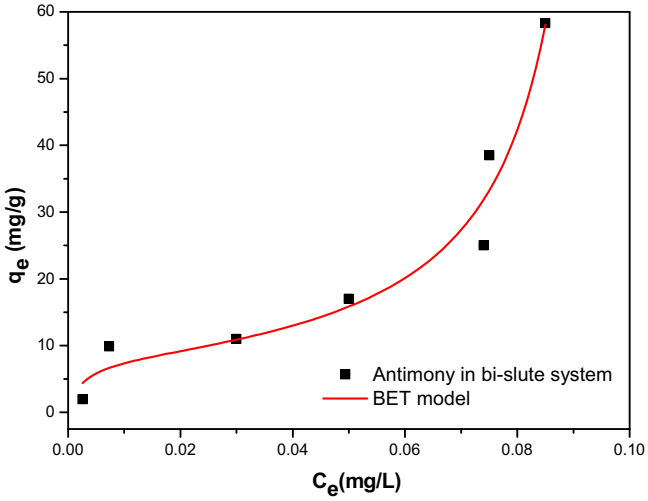

Fig. 6. BET adsorption isotherm of antimony onto DP/Ferrate in bi-solute system. $[Sb]_0$ ranged from 0.1 to 3 mg L^{-1}; $[As]_0$ = 1 mg L^{-1}; $[K_2FeO_4]$ = 50 mg L^{-1}; IS = 0.01 M; pH_0 = 4.0; 25 °C.

Compared to the spectrum of blank DP/Ferrate sample (Fig. 2(a)), a broader but less intense band at ~3400 cm^{-1} was observed in the As@DP/Ferrate (obtained at pH_0 6.5, Fig. 2(b)) sample owing to the deprotonation of the hydroxyl groups associated with Fe on the DP/Ferrate surface upon arsenic adsorption [44]. The bands at 1368 cm^{-1} and 1483 cm^{-1}, which were ascribed to the vibration of NO_3^- and CO_3^{2-}, were absent after arsenic adsorption, suggesting that $H_nAsO_4^{3-n}$ displaced the NO_3^- and CO_3^{2-} and promoted inner-sphere complexation [35]. A new peak appeared at 825 cm^{-1} that was not observed in the original spectrum of DP/Ferrate, evidencing the formation of new surface species. Jia et al. [35] verified that the band at ~825 cm^{-1} was attributed to the stretching vibration of As–O coordinating to iron atoms, i.e., As–O–Fe, of ferric arsenate precipitate on ferrihydrite. From the FTIR spectrum analysis, it can be concluded that arsenic was adsorbed onto DP/Ferrate via two steps: rapid ligand exchange between surface hydroxyl groups and $H_nAsO_4^{3-n}$ ions followed by a slow buildup of ferric arsenate surface precipitate [55].

By studying the IS dependence of antimony adsorption onto DP/Ferrate, it revealed that beyond pH 5.5, a combination of an outer-sphere complex ($FeOH_2^+ \ldots Sb(OH)_6^-$) and an inner-sphere complex ($Fe–OSb(OH)_5^-$) was promoted. To confirm the presence of these putative surface complexes, IR spectra of adsorbed antimony on the DP/Ferrate surface at pH_0 4.0 (Fig. 2(c)) and pH_0 6.5 (Fig. 2(d)) were studied. As illustrated in Fig. 2, both samples exhibited a loss of OH stretch vibrations of surface hydroxyl groups. The band at 460 cm^{-1} ascribed to Fe^{3+}–O^{2-} vibrational transition was decreased after adsorption for both samples. A new peak appeared at 598 cm^{-1} for Sb@DP/Ferrate (pH_0 4.0) and at 589 cm^{-1} for Sb@DP/Ferrate (pH_0 6.5), which was attributed to the Sb(V)–O stretching vibration [41,48]. It can be concluded that Fe–O–Sb bonding occurred in both samples. However, the differences in Sb surface complexes on DP/Ferrate at different pH can be identified from the IR spectra. The bands at 1479 cm^{-1} and 1364 cm^{-1}, which were assigned to NO_3^- and CO_3^{2-}, respectively, were absent in sample Sb@DP/Ferrate (pH_0 4.0). This was due to the displacement of NO_3^- and CO_3^{2-} by $Sb(OH)_6^-$ forming the inner-sphere complexes. Nevertheless, in the sample Sb@DP/Ferrate (pH_0 6.5), these two peaks were not absent but exhibited a downshift in wave number, suggesting the formation of outer-sphere surface complexes ($FeOH_2^+$–$NO_3^- \ldots Sb(OH)_6^-$).

Cooperative adsorption between As and Sb onto DP/Ferrate particles occurred. The IR spectrum of (As + Sb)@DP/Ferrate (obtained

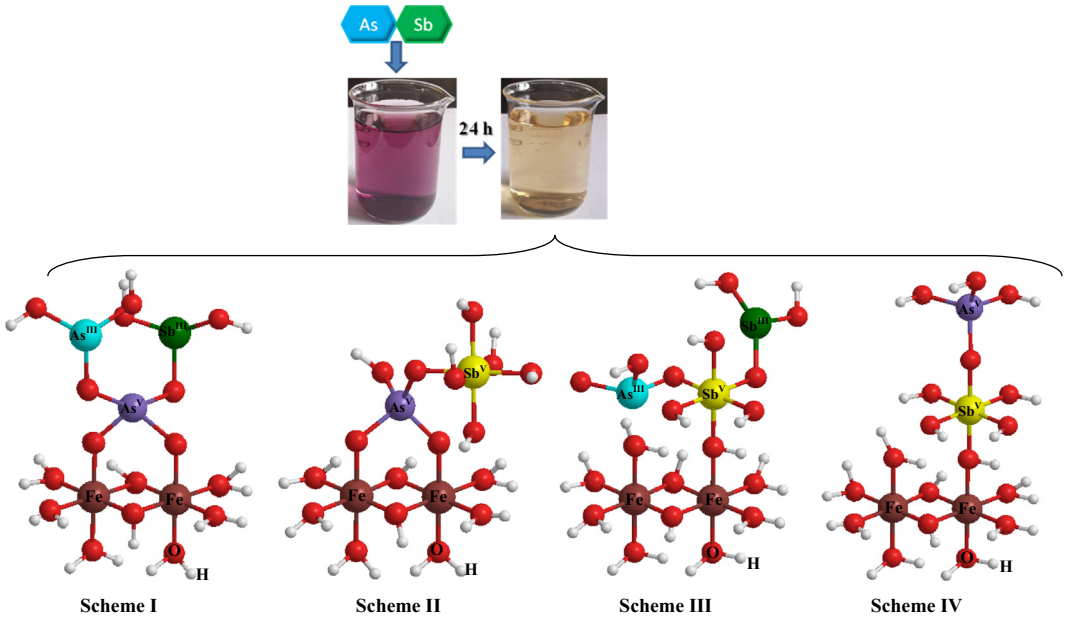

Fig. 7. Possible configurations of the surface structure of As and Sb on DP/Ferrate.

at pH_0 4.0, Fig. 2(e)) was investigated to understand the mechanism. It can be observed from Fig. 2 that the Sb(V)–O stretching vibration (~589 cm^{-1}) was present in the spectrum, whereas the As(V)–O stretching vibration shifted from 825 cm^{-1} to 819 cm^{-1} and was assigned to As–O–Sb bonds [56]. Therefore, the simple deduction that As(V) and Sb(V) were coordinated with the surface hydroxyl group independently was not adequate to clarify the synergistic sorption of As and Sb. Wang et al. [57,58] discovered the presence of arsenato antimonates precipitates during copper electro-refining. On the basis of Wang's work, we propose the following adsorption mechanism of As + Sb onto DP/Ferrate and illustrate in Fig. 7. In Scheme I and II, As(III) is oxidized to As(V) by Fe(VI) and adsorbed onto DP/Ferrate via bidentate binuclear complexation; i.e., two of the four As–O bonds are combined with iron atoms. In Scheme I, un-oxidized As(III) and Sb(III), before encountering ferrate, occupy the remaining two un-complexed As–O and form $AsAsO_4\downarrow$ or $SbAsO_4\downarrow$. In Scheme II, the un-complexed As–O bonds with $Sb(OH)_6^-$. In Scheme III and IV, a Sb(V) octahedron combines with an iron atom via monodentate interaction. Similarly, un-oxidized As(III) and Sb(III), and AsO_4 tetrahedra have the chance to share one edge with $Sb(OH)_6^-$. The above four schemes represent the possible existence of four units on the surface of DP/Ferrate. Nevertheless, these units would interconnect and produce a huge chain and three-dimensional structure.

To examine the postulated mechanism, XPS analysis of (As + Sb)@DP/Ferrate sample was conducted. Fig. 8(a) shows the As 3*d* core level photoelectron spectrum. One band centered at approximately 45.03 eV indicates that As(V) species were adsorbed onto the DP/Ferrate particle, whereas the other band centered at 43.87 eV suggested As(III) species were present on the surface of DP/Ferrate [29]. The results obtained from the XPS spectrum of As 3*d* were in accordance with Scheme I and III (Fig. 7) proposed in this study. The Sb 3*d* spectrum is illustrated in Fig. 8(b). The BE of Sb $3d_{3/2}$ was located at 541.8 eV. Using doublet separation, Sb $3d_{5/2}$ was located at 532.46 eV. It has been reported that the BE of Sb $3d_{3/2}$ in Sb_2O_5 and Sb_2O_3 was 540.8 eV and 539.6 eV, respectively [48]. Hence, the Sb species adsorbed onto the DP/Ferrate surface should be the other form of antimony compounds. According to XPS database [59], the dominant Sb species can be assigned to $K_3Sb_3As_2O_{14}{\cdot}5H_2O$. The FTIR and XPS results confirmed the formation of arsenato

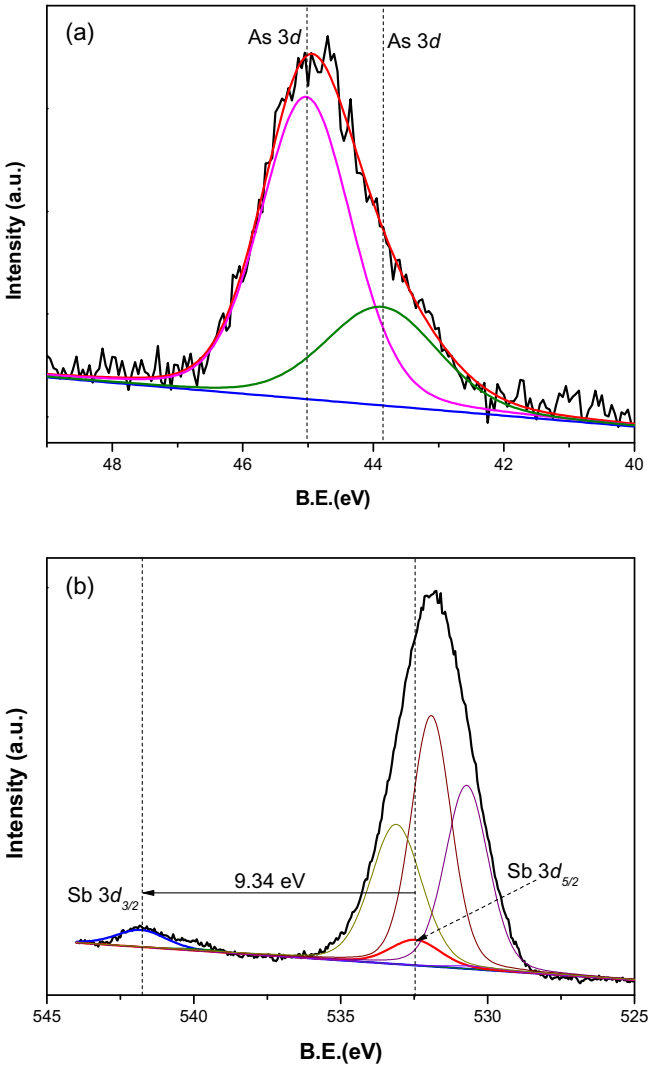

Fig. 8. High-resolution (a) As 3*d* and (b) Sb 3*d* core level photoelectron spectra of the (As + Sb)@DP/Ferrate obtained at pH_0 = 4.0.

antimonates on the DP/Ferrate surface, which was believed to be account for the synergistic promoting effect on simultaneous adsorption of As and Sb by DP/Ferrate.

4. Conclusion

This paper demonstrated that potassium ferrate is a viable water treatment agent to remediate arsenic and antimony combined pollution. Its decomposition product (DP/Ferrate) matched the characteristics of amorphous ferrihydrite. For single-solute sorption onto DP/Ferrate, the maximal adsorption capacity toward arsenic was 162.02 mg g^{-1} at pH_0 6.5 and toward antimony was 129.93 mg g^{-1} at pH_0 4.0, which were higher than those of ferrihydrite synthesized by rapid titration of ferric nitrate. For bi-solute sorption onto DP/Ferrate, the adsorption rates of As and Sb were both improved significantly compared to the single-solute system, demonstrating the occurrence of a synergistic effect between them. Furthermore, the diffusion of Sb within the porous structure of DP/Ferrate exhibited a marked enhancement in the presence of As. IR and XPS analyses were used to confirm surface speciation, and the key findings were: (1) for single-solute As adsorption, surface precipitation of ferric arsenate was observed; (2) for single-solute Sb adsorption, the spectral changes between pH 4.0 and 6.5 implied an inner-sphere complex as well as some outer-sphere adsorption; (3) for bi-solute (As + Sb) adsorption, the IR spectrum indicated the presence of As–O–Sb bonds and (in combination with the high-resolution XPS data) suggested the formation of arsenato antimonates across the surface of DP/Ferrate. On the basis of macroscopic experiments and the microscopic characteristics, the mechanism of simultaneous adsorption of As and Sb was postulated.

Acknowledgement

The authors are grateful for the financial support from the Science & Technology Office of Guangdong Province (Contract No. 2014A020216037).

Appendix A. Supplementary data

Supplementary data associated with this article can be found, in the online version, at http://dx.doi.org/10.1016/j.cej.2016.02.019.

References

[1] M.M. Rahman, K.C. Saha, S.C. Mukherjee, S. Pati, R.N. Dutta, S. Roy, Q. Quamruzzaman, M. Rahman, D. Chakraborti, Groundwater arsenic contamination in Bengal delta and its health effects, in: A.L. Ramanathan, S. Johnston, A. Mukherjee, B. Nath (Eds.), Safe and Sustainable Use of Arsenic-Contaminated Aquifers in the Gangetic Plain, Springer International Publishing, 2015, pp. 215–253.
[2] X. Guo, Z. Wu, M. He, X. Meng, X. Jin, N. Qiu, J. Zhang, Adsorption of antimony onto iron oxyhydroxides: adsorption behavior and surface structure, J. Hazard. Mater. 276 (2014) 339–345.
[3] C. Hansell, All manner of antimony, Nat. Chem. 7 (2015) 88.
[4] Council of the European Communities, Council Directive 76/464/EEC of 4 on pollution caused by certain dangerous substances discharged into the aquatic environment of the community, Off. J. L. 129 (1976) 23–29.
[5] USEPA, Water Related Fate of the 129 Priority Pollutants, vol. 1, USEPA, Washington, DC, 1979 (Doc. 745-R-00-007).
[6] G. Okkenhaug, Y.-G. Zhu, J. He, X. Li, L. Luo, J. Mulder, Antimony (Sb) and arsenic (As) in Sb mining impacted paddy soil from Xikuangshan, China: differences in mechanisms controlling soil sequestration and uptake in rice, Environ. Sci. Technol. 46 (2012) 3155–3162.
[7] P. Navarro, F.J. Alguacil, Adsorption of antimony and arsenic from a copper electrorefining solution onto activated carbon, Hydrometallurgy 66 (2002) 101–105.
[8] S.C. Wilson, P.V. Lockwood, P.M. Ashley, M. Tighe, The chemistry and behavior of antimony in the soil environment with comparisons to arsenic: a critical review, Environ. Pollut. 158 (2010) 1169–1181.
[9] G. Ungureanu, S. Santos, R. Boaventura, C. Botelho, Arsenic and antimony in water and wastewater: overview of removal techniques with special reference to latest advances in adsorption, J. Environ. Manage. 151 (2015) 326–342.
[10] D.G. Lumsdon, A.R. Fraser, J.D. Russell, N.T. Livesey, New infrared band assignments for the arsenate ion adsorbed on synthetic goethite (α-FeOOH), J. Soil Sci. 35 (1984) 381–386.
[11] S. Fendorf, M.J. Eick, P. Grossl, D.L. Sparks, Arsenate and chromate retention mechanisms on goethite. 1. Surface structure, Environ. Sci. Technol. 31 (1997) 315–320.
[12] K.P. Raven, A. Jain, H.L. Loeppert, Arsenite and arsenate adsorption on ferrihydrite: kinetics, equilibrium, and adsorption envelopes, Environ. Sci. Technol. 32 (1998) 344–349.
[13] M.L. Farquhar, J.M. Charnock, F.R. Livens, D.J. Vaughan, Mechanisms of arsenic uptake from aqueous solution by interaction with goethite, lepidocrocite, mackinawite, and pyrite: an X-ray absorption spectroscopy study, Environ. Sci. Technol. 36 (2002) 1757–1762.
[14] E.A. Deliyanni, D.N. Bakoyannakis, A.I. Zouboulis, K.A. Matis, Sorption of As(V) ions by akaganéite-type nanocrystals, Chemosphere 50 (2003) 155–163.
[15] J. Giménez, M. Martínez, J. Pablo, M. Rovira, L. Duro, Arsenic sorption onto natural hematite, magnetite, and goethite, J. Hazard. Mater. 141 (2007) 575–580.
[16] E.D. Burton, R.T. Bush, S.G. Johnston, K.M. Watling, R.K. Hocking, L.A. Sullivan, G.K. Parker, Sorption of arsenic (V) and arsenic (III) to schwertmannite, Environ. Sci. Technol. 43 (2009) 9202–9207.
[17] J. Zhu, M. Pigna, V. Cozzolino, A.G. Caporale, A. Violante, Sorption of arsenite and arsenate on ferrihydrite: effect of organic and inorganic ligands, J. Hazard. Mater. 189 (2011) 564–571.
[18] A. Jain, K.P. Raven, R.H. Loeppert, Arsenite and arsenate adsorption on ferrihydrite: surface charge reduction and net OH^- release stoichiometry, Environ. Sci. Technol. 33 (1999) 1179–1184.
[19] N. Zhang, P. Blowers, J. Farrell, Evaluation of density functional theory methods for studying chemisorptions of arsenite on ferric hydroxides, Environ. Sci. Technol. 39 (2005) 4816–4822.
[20] G.A. Waychunas, B.A. Rea, C.C. Fuller, J.A. Davis, Surface chemistry of ferrihydrite: part 1 EXAFS studies of the geometry of coprecipitated and adsorbed arsenate, Geochim. Cosmochim. Acta 57 (1993) 2251–2269.
[21] X. Sun, H.E. Doner, An investigation of arsenate and arsenite bonding structures on goethite by FTIR, Soil Sci. 161 (1996) 865–872.
[22] G.A. Waychunas, C.C. Fuller, B.A. Rea, J.A. Davis, Wide angle X-ray scattering (WAXS) study of "two-line" ferrihydrite structure: effect of arsenate sorption and counterion variation and comparison with EXAFS results, Geochim. Cosmochim. Acta 60 (1996) 1765–1781.
[23] A.C. Scheiost, A. Rossberg, D. Vantelon, I.O. Xifra, R. Kretzschmar, A.-K. Leuz, H. Funke, C.A. Johnson, Quantitative antimony speciation in shooting-range soil by EXAFS spectroscopy, Geochim. Cosmochim. Acta 70 (2006) 3299–3312.
[24] S. Mitsunobu, T. Harada, Y. Takahashi, Comparison of antimony behavior with that of arsenic under various soil redox conditions, Environ. Sci. Technol. 40 (2006) 7270–7276.
[25] V.K. Sharma, Potassium ferrate(VI): an environmentally friendly oxidant, Adv. Environ. Res. (Oxford, UK) 6 (2002) 143–156.
[26] V.K. Sharma, Oxidation of inorganic compounds by ferrate (VI) and ferrate (V): one-electron and two-electron transfer steps, Environ. Sci. Technol. 44 (2010) 5148–5152.
[27] Y. Jiang, J.E. Goodwill, J.E. Tobiason, D.A. Reckhow, Effect of different solutes, natural organic matter, and particulate Fe(III) on ferrate (VI) decomposition in aqueous solutions, Environ. Sci. Technol. 2015 (9) (2015) 2841–2848.
[28] Y. Lee, I.H. Um, J. Yoon, Arsenic (III) oxidation by iron (VI) (ferrate) and subsequent removal of arsenic (V) by iron (III) coagulation, Environ. Sci. Technol. 37 (2003) 5750–5756.
[29] R. Prucek, J. Tuček, J. Kolařík, J. Filip, Z. Marušák, V.K. Sharma, R. Zbořil, Ferrate (VI)-induced arsenite and arsenate removal by in situ structural incorporation into magnetic iron (III) oxide nanoparticles, Environ. Sci. Technol. 47 (2013) 3283–3292.
[30] M. Johnson, B. Lorenz, Antimony remediation using ferrate (VI), Sep. Sci. Technol. 50 (2015) 1611–1615.
[31] C. Shan, Z. Ma, M. Tong, Efficient removal of trace antimony (III) through adsorption by hematite modified magnetic nanoparticles, J. Hazard. Mater. 268 (2014) 229–236.
[32] L. Delaude, P. Laszlo, A novel oxidizing reagent based on potassium ferrate (VI), J. Org. Chem. 61 (1996) 6360–6370.
[33] J.L. Jambor, J.E. Dutrizac, Occurrence and constitution of natural and synthetic ferrihydrite, a widespread iron oxyhydroxide, Chem. Rev. 98 (1998) 2549–2585.
[34] J.D. Russell, Infrared spectroscopy of ferrihydrite: evidence for the presence of structural hydroxyl groups, Clay Miner. 1 (1979) 109–114.
[35] Y. Jia, L. Xu, X. Wang, G.P. Demopoulos, Infrared spectroscopic and X-ray diffraction characterization of the nature of adsorbed arsenate on ferrihydrite, Geochim. Cosmochim. Acta 71 (2007) 1643–1654.
[36] M. Ristić, E. De Grave, S. Musić, S. Popović, Z. Orehovec, Transformation of low crystalline ferrihydrite to α-Fe_2O_3 in the solid state, J. Mol. Struct. 834–836 (2007) 454–460.
[37] J.A. Davis, J.O. Leckie, Surface ionization and complexation at the oxide/water interface. II. Surface properties of amorphous iron oxyhydroxide and adsorption of metal ions, J. Colloid Interface Sci. 67 (1978) 90–107.
[38] J.A. Davis, D.B. Kent, Surface complexation modeling in aqueous geochemistry, Rev. Mineral. 23 (1990) 177–260.

[39] D. Peak, T. Regier, Direct observation of tetrahedrally coordinated Fe(III) in ferrihydrite, Environ. Sci. Technol. 46 (2012) 3163–3168.
[40] S. Dixit, J.G. Hering, Comparison of arsenic (V) and arsenic (III) sorption onto iron oxide minerals: implications for arsenic mobility, Environ. Sci. Technol. 37 (2003) 4182–4189.
[41] M. Vithanage, A.U. Rajapaksha, X. Dou, N.S. Bolan, J.E. Yang, Y.S. Ok, Surface complexation modeling and spectroscopic evidence of antimony adsorption on iron-oxide-rich red earth soils, J. Colloid Interface Sci. 406 (2013) 217–224.
[42] A.-K. Leuz, H. Mönch, C.A. Johnson, Sorption of Sb(III) and Sb(V) to goethite: influence on Sb(III) oxidation and mobilization, Environ. Sci. Technol. 40 (2006) 7277–7282.
[43] J. Xi, M. He, C. Lin, Adsorption of antimony (V) on kaolinite as a function of pH, ionic strength and humic acid, Environ. Earth Sci. 60 (2010) 715–722.
[44] K.A. McComb, D. Craw, A.J. McQuillan, ATR-IR spectroscopic study of antimonite adsorption to iron oxide, Langmuir 23 (2007) 12125–12130.
[45] L. Axe, P.R. Anderson, Sr diffusion and reaction within Fe oxides: evaluation of the rate-limiting mechanism for sorption, J. Colloid Interface Sci. 175 (1995) 157–165.
[46] Z. Wen, C. Dai, Y. Zhu, Y. Zhang, Arsenate removal from aqueous solutions using magnetic mesoporous iron manganese bimetal oxides, RSC Adv. 5 (2015) 4058–4068.
[47] X. Dou, X. Yu, B. Zhao, Y. Zhang, X. Ji, A performance comparison of arsenate removal from water by five iron oxides, Chin. J. Environ. Eng. 4 (2010) 1989–1994.
[48] W. Xu, H.J. Wang, R.P. Liu, X. Zhao, J.H. Qu, The mechanism of antimony (III) removal and its reactions on the surfaces of Fe–Mn binary oxide, J. Colloid Interface Sci. 363 (2011) 320–326.
[49] X.H. Li, X.M. Dou, J.Q. Li, Antimony (V) removal from water by iron zirconium bimetal oxide: performance and mechanism, J. Environ. Sci. China 24 (2012) 1197–1203.
[50] X.Q. Wang, M.C. He, C.Y. Lin, Y.X. Gao, L. Zheng, Antimony (III) oxidation and antimony (V) adsorption reactions on synthetic manganite, Chem. Erde Geochem. 72 (2012) 41–47.
[51] F. Kolbe, H. Weiss, P. Morgenstern, R. Wennrich, W. Lorenz, K. Schurk, H. Stanjek, B. Daus, Sorption of aqueous antimony and arsenic species onto akaganeite, J. Colloid Interface Sci. 357 (2011) 460–465.
[52] A. Jain, R.H. Loeppert, Effect of competing anions on the adsorption of arsenate and arsenite by ferrihydrite, J. Environ. Qual. 29 (2000) 1422–1430.
[53] A. Violante, M. Pigna, Competitive sorption of arsenate and phosphate on different clay minerals and soils, Soil Sci. Soc. Am. J. 66 (2002) 1788–1796.
[54] C.H. Giles, D. Smith, A. Huitson, A general treatment and classification of the solute adsorption isotherm. I: theoretical, J. Colloid Interface Sci. 47 (1974) 755–765.
[55] H. Zhao, R. Stanforth, Competitive adsorption of phosphate and arsenate on goethite, Environ. Sci. Technol. 35 (2001) 4753–4757.
[56] S.C.B. Myneni, S.J. Traina, G.A. Waychunas, T.J. Logan, Experimental and theoretical vibrational spectroscopic evaluation of arsenate coordination in aqueous solutions, solids, and at mineral-water interfaces, Geochim. Cosmochim. Acta 62 (1998) 3285–3300.
[57] X.W. Wang, Study on the mechanism of the formation and action of arsenate antimonic acid in copper electrorefining (Ph.D. Dissertation), Central South University, Changsha, 2003 (in Chinese).
[58] X.W. Wang, Q.Y. Chen, Z.L. Yin, L.S. Xiao, Identification of arsenate antimonates in copper anode slimes, Hydrometallurgy 84 (2006) 211–217.
[59] J.F. Moulder, W.F. Stickle, P.E. Sobol, Handbook of X-ray Photoelectron Spectroscopy, Perkin-Elmer Corporation Publisher, Montreal, 1992, pp. 617–624.